A novel deamido-NAD$^+$-binding site revealed by the trapped NAD-adenylate intermediate in the NAD$^+$ synthetase structure

Menico Rizzi[1,2]*, Martino Bolognesi[3] and Alessandro Coda[2]

Background: Nicotinamide adenine dinucleotide (NAD$^+$) has a central role in life processes. The ubiquitous enzyme NAD$^+$ synthetase catalyzes a key step in NAD$^+$ biosynthesis, transforming deamido-NAD$^+$ into NAD$^+$ by a two-step reaction. NAD$^+$ synthetase belongs to the amidotransferase family and has been recognized as a member of the family of N-type ATP pyrophosphatases. In order to investigate the mechanism of the reaction carried out by NAD$^+$ synthetase we have determined a high-resolution three-dimensional structure of the *Bacillus subtilis* homodimeric NAD$^+$ synthetase in complex with the trapped reaction intermediate NAD-adenylate.

Results: Two NAD-adenylate molecules and two pyrophosphate (PP_i) molecules are observed in the 1.3 Å resolution structure of the NAD$^+$ synthetase–NAD-adenylate complex. Structural studies on the NAD$^+$ synthetase–NAD-adenylate adduct and on the cation-binding sites reveal a new deamido-NAD$^+$-binding site located at the subunit interface, locate a binuclear magnesium cluster at the ATP-binding site and, identify two monovalent cation sites, one of which may represent an ammonium-binding site.

Conclusions: Our results suggest that two different catalytic strategies have been adopted by NAD$^+$ synthetase in the two different steps of the reaction. During the adenylation step, no protein residues seem to be located properly to directly participate in catalysis, which is likely to be carried out with the fundamental assistance of an electron-withdrawing trimetallic constellation present in the active site. A different behavior is observed for the second step, in which an ammonium ion is the binding species. In this step, Asp173 is a key residue in both deprotonation of the primarily bound ammonium ion, and stabilization of the tetrahedral transition-state intermediate. Moreover, the structural data suggest that product release can take place only after all substrates are bound to the enzyme, and product release is ultimately controlled by the conformation adopted by two mobile loops.

Addresses: [1]Department of Pharmaceutical Science and Technology, University of Torino, via Pietro Giuria 9, 10125 Torino, Italy, [2]Department of Genetics and Microbiology, University of Pavia, via Abbiategrasso 207, 27100 Pavia, Italy and [3]Department of Physics and IST - Advanced Biotechnology Centre, University of Genova, Largo R. Benzi, 16136 Genova, Italy.

*Corresponding author.
E-mail: rizzi@ipvgen.unipv.it

Key words: amidotransferase, NAD(P) binding, NAD$^+$ synthetase, cation-containing active site

Received: **15 May 1998**
Revisions requested: **8 July 1998**
Revisions received: **15 July 1998**
Accepted: **16 July 1998**

Structure 15 September 1998, **6**:1129–1140
http://biomednet.com/elecref/0969212600601129

Introduction

Nicotinamide adenine dinucleotide (NAD$^+$) and its phosphorylated form (NADP$^+$) are essential and ubiquitous coenzymes, which play a fundamental role in metabolism. They are involved in biochemical processes ranging from redox reactions to DNA repair, DNA recombination and protein–ADP ribosylation. Thus, NAD$^+$ biosynthesis is a vital metabolic pathway in all living organisms. The coenzyme biosynthesis can be pursued through a *de novo* pathway or through a pyridine nucleotide salvage pathway that allows NAD$^+$ recycling [1–3].

NAD$^+$ synthetase (EC 6.3.5.1) catalyzes the last step in NAD$^+$ biosynthesis, transforming deamido-NAD$^+$ into the final product NAD$^+$ by a two step reaction: the enzyme activates deamido-NAD$^+$ via the formation of NAD-adenylate (NAD-ad), in the presence of Mg–ATP; a nucleophilic ammonia molecule then attacks the adenylate intermediate leading to NAD$^+$ ([4]; Figure 1).

Mutants of *Bacillus subtilis* NAD$^+$ synthetase with altered activity were shown to be severely affected in cellular functionality [5,6]. Moreover, it has been reported recently that the enzyme is strongly induced in response to general stress conditions, suggesting a possible involvement as a stress-response protein [7].

NAD$^+$ synthetase belongs to the extensively studied amidotransferase family, whose members are involved in a variety of biochemical processes [8]. Amidotransferases are characterized by the presence of two distinct domains, which may either belong to the same polypeptide chain or exist as independent subunits. A glutamine amide-transfer domain (GAT) is responsible for the ability to use glutamine as a nitrogen source, whereas a synthetase/synthase domain confers the specificity and catalyzes the transfer of ammonia to the substrate. Amidotransferases can be grouped into two families depending on their GAT domain: G-type amidotransferases, having a Cys–His–Glu catalytic

Figure 1

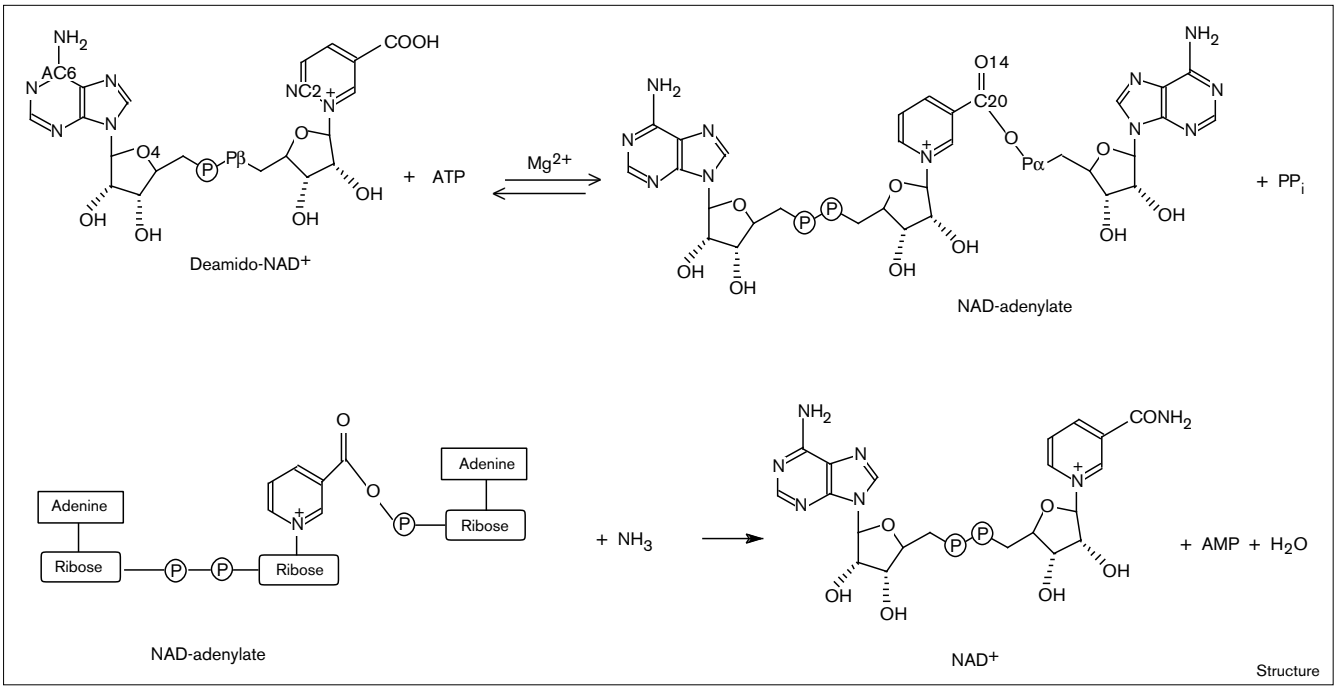

A scheme of the two-step reaction catalyzed by NAD^+ synthetase.

triad, and F-type or Ntn (N-terminal nucleophile) amidotransferases, which display a strictly conserved N-terminal cysteine [8]. Within the two families, the three-dimensional structures of phosphorybosilpyrophosphate (PRPP) amidotransferase [9], GMP synthetase [10], NAD^+ synthetase [11], glucosamine 6-phosphate synthase [12], carbamoylphosphate synthetase [13] and asparagine synthetase [14] have been reported. Details from these crystallographic analyses have partly unraveled the molecular bases for catalytic mechanisms in amidotransferases [8].

NAD^+ synthetase from *B. subtilis* has been characterized previously and reported to be strictly ammonia dependent for its catalytic activity, even though the existence of an independent subunit bearing the GAT domain has not been completely ruled out [6]. On the other hand, the enzyme from *Mycobacterium tuberculosis*, a 738-residue polypeptide chain, has been isolated recently and shown to be able to use both ammonia and glutamine as nitrogen sources [15]. Furthermore, both the human and tobacco NAD^+ synthetases have been reported to use glutamine as a nitrogen source [16,17].

The structures of NAD^+ synthetase from *B. subtilis*, in its free form and in complex with ATP, have been previously reported [11]. Each subunit within the functional homodimer adopts an α/β open sheet topology, closely related to the well known Rossmann fold. The ATP-binding site is located entirely within one subunit at the α/β open sheet topological switch point, whereas the putative deamido-NAD^+-binding site was proposed to be located at the subunit interface, where an additional, uncleaved, ATP molecule was observed [11]. An early proposal that NAD^+ synthetase, GMP synthetase, asparagine synthetase and argininosuccinate synthetase form a new class of N-type ATP pyrophosphatases (ATP PPases), characterized by the strictly conserved fingerprint sequence Ser–Gly–Gly–X–Ser/Thr–Ser/Thr (where X is any amino acid) at the P-loop [10], has been confirmed by comparison of the three-dimensional structures of NAD^+ synthetase and GMP synthetase. Indeed NAD^+ synthetase and the ATP PPase domain of GMP synthetase are closely related (with a root mean square deviation [rmsd] of 1.6 Å for 116 Cα pairs), revealing striking structural relationships at the ATP-binding site [11].

Recently, Savage *et al.* [18] have observed a remarkable structural similarity amongst NAD^+ synthetase, the PPase domain of GMP synthetase, and phosphadenylyl sulfate (PAPS) reductase. PAPS reductase converts phosphadenylyl sulfate into phospho-adenosine-phosphate, and does not display any ATPase activity; nevertheless it shares ~30% sequence identity with ATP sulphorylases from different organisms [18]. Taken together, these observations suggest that N-type ATP PPases, ATP sulphorylases and PAPS reductases may have evolved from a

common ancestral nucleotide-binding protein, and can be grouped into a new family of enzymes endowed with nucleotide α-hydrolase activity [18].

Here, we report the three-dimensional structure of the complex formed by *B. subtilis* NAD+ synthetase and the trapped reaction intermediate NAD-ad (E–NAD-ad), at 1.3 Å resolution. Our results reveal, at high resolution, a new deamido-NAD+-binding site at the enzyme dimer interface, confirming previous proposals, locate a binuclear magnesium cluster at the ATP-binding site, and locate two monovalent cation sites, one of which is a potential candidate for an ammonium ion binding site.

As a consequence of the vital involvement of NAD+ in metabolism, the coenzyme biosynthetic pathway is a natural candidate for the design of drugs against pathogenic organisms, and NAD+ synthetase may be considered a target for the development of a new class of antibiotics. The structure of the E–NAD-ad complex, reported here, may serve as an ideal guide for the rational design of selective and efficient enzyme synthetic inhibitors.

Results

The three-dimensional structure of the NAD-ad intermediate bound to the enzyme is reported in the present study; we therefore consider the deamido-NAD+ and AMP moieties of NAD-ad to analyze the substrate-binding site and the cation-binding sites, and to discuss the catalytic mechanism. We observed two NAD-ad and two pyrophosphate (PP_i) molecules in the dimeric enzyme, in keeping with the local dyad relating the two subunits in the functional homodimer. Residues from the two subunits in NAD+ synthetase are numbered A1–A271 and B1–B271, respectively, and the reported distances refer to the A subunit.

The deamido-NAD+-binding site

The structural determinants involved in NAD(P) recognition for a large number of NAD(P)-binding proteins, have been reviewed extensively [19,20]. According to the Structural Classification of Proteins database, the folds observed so far in a variety of NAD(P)-binding proteins, are distributed between three major classes: all-β, α+β and α/β topologies [21]. Within the α/β class, the most frequently observed is the dinucleotide-binding fold, also called the Rossmann fold [22], which is adopted by a large number of enzymes using NAD(P) as a redox cofactor. The two peculiar features of a canonical Rossmann fold are represented by the Gly–X–Gly–X–X–Gly sequence fingerprint (the glycine-rich loop), and by a βαβ motif, which contacts the dinucleotide diphosphate moiety.

Although the *B. subtilis* NAD+ synthetase subunit consists of a single α/β domain, whose topological organization closely resembles the dinucleotide-binding domain [11], deamido-NAD+ does not bind in proximity to the βαβ motif at the C-terminal edge of the parallel β sheet. Instead, the deamido-NAD+-binding site is located at the subunit interface, where an extended cleft is defined by the quaternary structure of NAD+ synthetase (Figure 2). The deamido-NAD+ adenylyl end is positioned close to the N terminus of the two S4 and S5 β strands of one subunit and close to the C-terminal extension of the other (residues 260–268; Figure 2). The adenyne-ribose (*A*-ribose), diphosphate, nicotinic-ribose (*N*-ribose) and nicotinic moieties, are sandwiched between the H6 helices provided by the two subunits on one side and by the H12 C-terminal helix and the 166–175 loop (both from the same subunit) on the other side (Figure 2). The dinucleotide adopts an extended conformation at both the adenine and nicotinic ends: the distances *A*C6–*N*C2 and Pβ–*N*C2 are 16.93 Å and 6.66 Å, respectively, and are in good agreement with the reported values for enzyme-bound NAD(P), where the dinucleotide has an open conformation ([20]; Figures 1, 2 and 3a).

Inspection of the residues surrounding the deamido-NAD+ moiety (as observed in the bound NAD-ad) reveals a new deamido-NAD+ binding mode. The adenosyl part is observed in the *anti* conformation, clamped by LeuB153 and HisA257, which fix its position (Figure 3a). The resulting orientation allows the formation of hydrogen bonds between the adenosyl N1 atom and the hydroxyl group of TyrB32 (2.70 Å) and between the adenosyl N3 atom and the Nζ atom of LysA170 (3.24 Å). The diol moiety of the *A*-ribose, is engaged in four hydrogen bonds with the water molecules W458 (2.72 Å), W438 (2.83 Å) and W379 (2.74 Å) and AspB177 (2.68 Å; see Figure 3a). The latter interaction (by an aspartate more frequently than a glutamate) is invariably observed in NAD+-binding proteins, representing a contribution to the thermodynamics of NAD+ binding, as well as a selective factor in discriminating against NADP+ binding [19]. Remarkably, the *A*-ribose O4 atom (as labeled in Figure 1) makes a hydrogen bond with the Nε2 atom of HisA257 (3.26 Å), one of the two residues fixing the adenosyl moiety in its position (Figures 1 and 3a).

The diphosphate moiety of deamido-NAD+ does not make a hydrogen bond with the mainchain atoms of the glycine-rich motif, as instead occurs for NAD(P), in canonical Rossmann folds [19]. Conversely, the disphosphate moiety is stabilized strongly by a series of salt bridges and hydrogen bonds with positively charged residues. In particular, the diphosphate terminal oxygen atoms are hydrogen bonded to ArgA137 (2.72 Å) and LysA258 (2.80 Å; see Figure 3a). As observed for the *A*-ribose diol oxygen atoms, an acidic residue, GluA223, hydrogen bonds the *N*-ribose diol oxygen atoms at 2.70 Å and 2.72 Å, respectively (Figure 3a).

The orientation of the nicotinic-acid moiety is determined by contacts with PheA167 and ThrA169, located on opposite sides of the pyridinic ring (Figure 3a). Moreover,

Figure 2

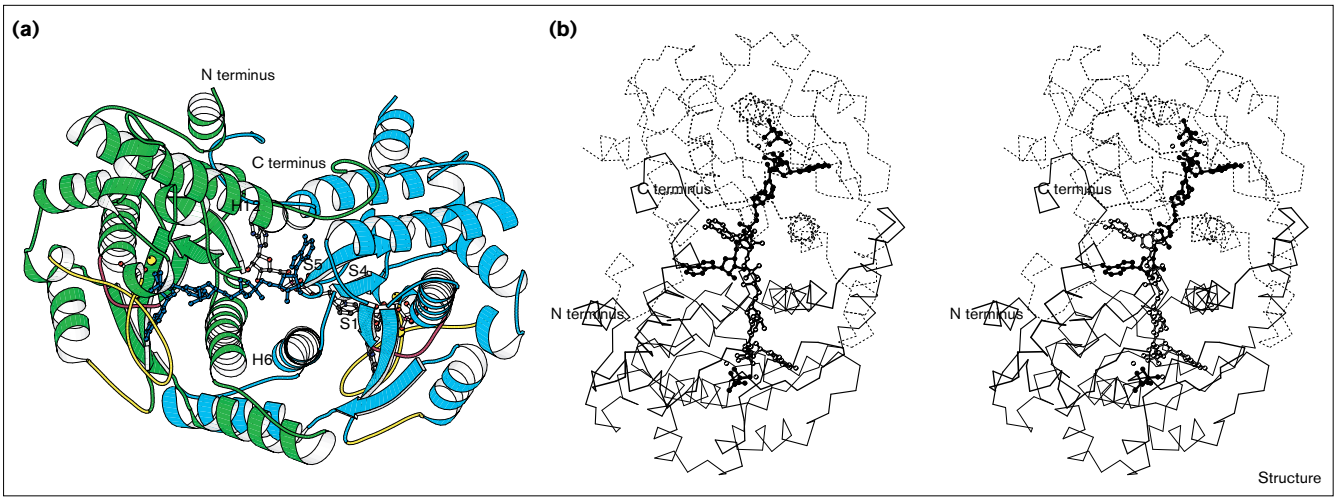

The dimer of NAD^+ synthetase. **(a)** Ribbon representation of the dimer viewed perpendicular to the local dyad. The A and B subunits are colored in cyan and light green, respectively. The NAD-ad and PP_i molecules are shown in ball-and-stick representation and Mg^{2+} ions are depicted as yellow spheres. Oxygen atoms are colored in red, nitrogen atoms in dark blue, carbon atoms in gray and phosphorus atoms in magenta. One of the two NAD-ad molecules is entirely colored in dark blue. The two mobile loops undergoing structural reorganization upon substrate binding, are shown as a yellow coil. The 'P-loop' is colored in violet. **(b)** Stereoview of the Cα trace of the dimer of NAD^+ synthetase. The A and B subunits are drawn with continuous and dashed lines, respectively. NAD-ad and PP_i are shown in ball-and-stick representation and Mg^{2+} ions are shown as spheres. This figure was generated using MOLSCRIPT [43].

AspA173 may contribute to the proper orientation of the nicotinic carboxylate, to direct the nucleophilic attack on the α-phosphorous of ATP, during the first step of the catalyzed reaction (Figure 1). In fact, the nicotinic carboxylate moiety of deamido-NAD^+ may be blocked in the observed conformation by the electrostatic repulsion of AspA173 (Figure 3a).

The ATP-binding site and the binuclear magnesium cluster

Within each NAD^+ synthetase subunit the ATP-binding site is located at the topological switch point, between the first (S1) and the fourth (S4) parallel β strands, as previously reported ([11]; Figure 2).

In the structure of the E–NAD-ad complex a PP_i molecule and the AMP moiety of NAD-ad occupy the ATP-binding site, adopting the same overall structure observed in the E–ATP adduct ([11]; Figures 2 and 3b). The AMP adenine ring is stabilized by hydrogen bonds between the N6 atom and the Oδ1 atom of GlnA84 (2.86 Å) and by the N3 atom and the NH_2 atom of ArgA78 (3.05 Å; see Figure 3b). Moreover, it provides a stacking interaction with the guanidino group of ArgA139 (with a shortest contact distance of 3.44 Å). The ribose diol oxygen atoms are both engaged in hydrogen bonds: one with residue ThrA157 (2.72 Å), the second with water W321 (2.76 Å) and with the carbonyl atom of GlyA44 (2.69 Å; Figure 3b). The PP_i anion (the leaving group in the first step of the catalyzed reaction), is partially stabilized through interactions with residues of the P-loop. In particular SerA46 and SerA51 Oγ atoms are hydrogen bonded with the β-phosphate oxygen atoms (2.68 Å and 2.78 Å, respectively), and the GlnA49 mainchain nitrogen atom is engaged in a hydrogen bond with the βγ-bridge oxygen atom (3.35 Å). A strong salt bridge is established between the γ-phosphate and residue LysA186 (2.71 Å). A further contribution to PP_i binding is provided by the dipole of the H3 helix, whose N terminus is centered on the βγ-bridge oxygen atom (Figure 3b).

An F_o–F_c difference Fourier map, calculated after crystallographic refinement, showed two strong electron density peaks located between the AMP moiety of NAD-ad and PP_i units; the peaks were interpreted as magnesium ions, considering the composition of the crystallization medium and the observed octahedral coordination typical of Mg^{2+} [23]. These two peaks were definitively assigned to a Mg^{2+} pair following difference Fourier analysis, at 2.5 Å resolution, on a crystal of the E–ATP complex, soaked in 0.05 M Mn^{2+}. Two strong peaks (> 10σ above the rms electron density) were located at the same sites provisionally interpreted as Mg^{2+} ions in the E–NAD-ad adduct. The two Mg^{2+} ions are referred to as Mg(I) and Mg(II). The Mg(I) ligands are provided by the AspA50 Oδ2 atom (2.09 Å), the GluA162 Oε2 atom (2.10 Å), the PP_i γ-phosphate and β-phosphate oxygen atoms at 2.09 Å and 2.10 Å, respectively, and the AMP α-phosphate O1α atom (2.05 Å; Figure 3c). The coordination sphere is completed by W665 at a distance of 2.05 Å. Mg(II) is also octahedrally coordinated by the AMP α-phosphate O3α atom (2.01 Å),

Figure 3

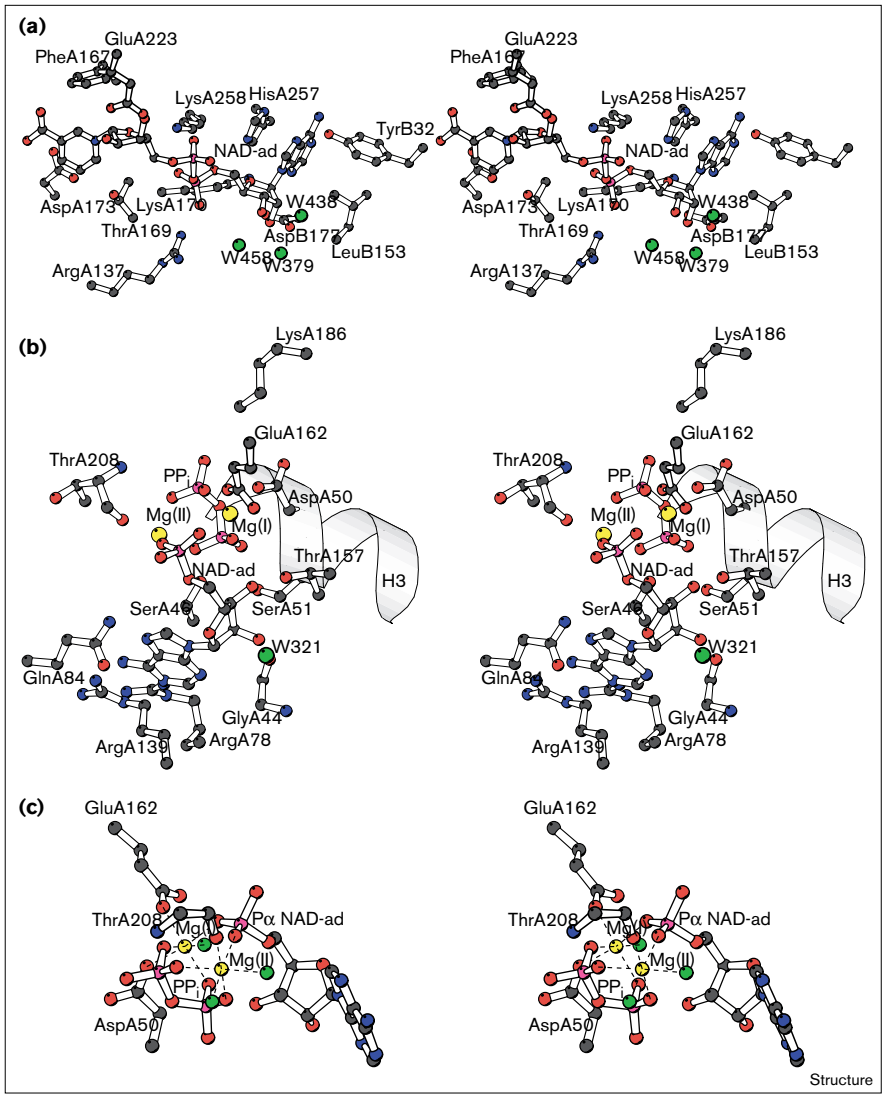

Figure 3

The deamido-NAD+ and ATP-binding sites. **(a)** Stereoview of the deamido-NAD+-binding site. Only the deamido-NAD+ portion of the NAD-ad intermediate is shown. The adenine (*A*) and nicotinic (*N*) ends are on the right-hand and left-hand sides, respectively. **(b)** Stereoview of the ATP-binding site. The PP_i molecule, two Mg^{2+} cations and the AMP portion of NAD-ad intermediate, are shown. **(c)** Stereoview of the Mg^{2+} binuclear cluster at the ATP-binding site. Again the PP_i molecule, the two Mg^{2+} cations and the AMP portion of NAD-ad are shown. Dashed lines connect Mg^{2+} ions to the respective coordinative ligands. The color coding is as described in Figure 2. Water molecules are shown as green spheres. This figure was generated using MOLSCRIPT [43].

the PP_i β-phosphate and γ-phosphate oxygen atoms, at 2.07 Å and 2.06 Å, respectively, two water molecules, W666 (2.10 Å) and W667 (2.11 Å), and the carbonyl atom of ThrA208 (2.10 Å; Figure 3c).

The monovalent cation-binding sites

It has been reported that K^+ is an essential component for optimal NAD+ synthetase activity [6,24]. In order to discover possible monovalent cation-binding sites in NAD+ synthetase, we collected X-ray diffraction data from one crystal of the E–ATP adduct soaked in a solution saturated with thallium acetate. The electron-dense Tl^+ cation has previously been employed to investigate monovalent cation-binding sites in proteins, in particular as a substitute for K^+ and NH_4^+ species ([25] and references therein). An example of such an application is provided by glutamine synthetase, which catalyzes the ATP-dependent condensation of ammonia and glutamate to produce glutamine and ADP [25,26].

Inspection of the difference Fourier map of the E–ATP–Tl^+ complex revealed two strong peaks in proximity to the bound pyrophosphate, at the ATP-binding site. These peaks were present in both subunits with comparable heights (15σ above the rms electron density) and have been referred to as M^+(I) and M^+(II). Remarkably, in the structure of the E–NAD-ad complex, the positions occupied by the two electron-dense Tl^+ cations are occupied by two solvent molecules. All the distances and geometries quoted here refer to the position of these two water molecules in the E–NAD-ad adduct.

M^+(I), which is replaced by water molecule W559 in the E–NAD-ad complex, is at a distance of 2.77 Å from the

Figure 4

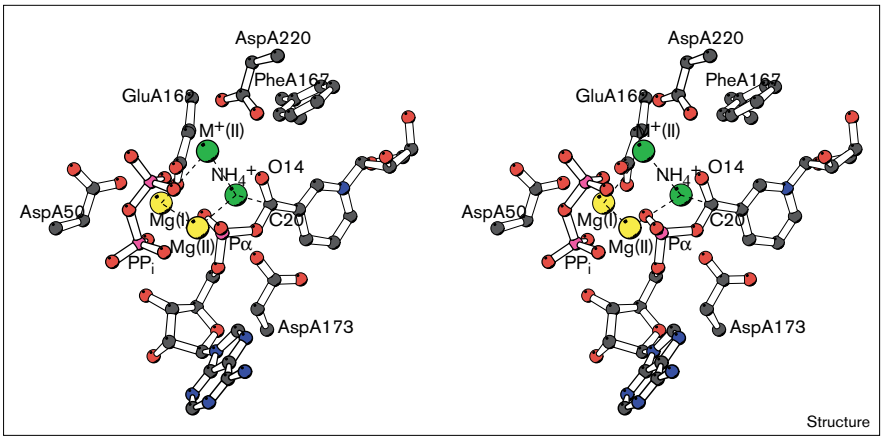

Stereoview of the monovalent cation-binding sites. In the text, the NH_4^+ is reported as M^+(I). Dashed lines connect the trimetallic constellation and the ammonium ion. Only a portion of NAD-ad, containing the AMP moiety and part of the deamido-NAD^+ moiety, is shown. Color coding is as described in Figures 2 and 3. This figure was generated using MOLSCRIPT [43].

NAD-ad nicotinic C20 atom, the angle M^+(I)–C20–O14 being 97.6° (Figure 4). Because C20 is the electrophile attacked from the incoming base in the second step of the catalyzed reaction, M^+(I) is likely to represent an ammonium-binding site in NAD^+ synthetase. A complex network of electrostatic interactions participate in the stabilization of M^+(I). Amongst them, the PheA167 carbonyl oxygen atom is at a distance of 2.59 Å, and the O1α atom of the AMP α-phosphate is at 3.06 Å, whereas two other important salt bridges are established with GluA163 and AspA173, which are at 3.41 Å and 2.73 Å, respectively (Figure 4). Interestingly, both AMP α-phosphate oxygen atoms and GluA162 are already engaged in Mg(I) coordination, thus playing a remarkable role in cation stabilization in NAD^+ synthetase. In keeping with our proposal that this monovalent cation-binding site might represent the ammonium-binding site, the coordination observed for M^+(I) is approximately tetrahedral, as could be expected for an ammonium ion.

The second monovalent cation-binding site, M^+(II) (occupied by the water molecule W339 in the E–NAD-ad adduct), is located in the ATP-binding site, close to the PP_i molecule. Again, a number of electrostatic interactions with M^+(II) are observed: the PP_i O1γ and O3γ atoms are at 2.54 Å and 3.46 Å, respectively, the AMP α-phosphate O1α and O3α oxygen atoms are at 3.14 Å and 3.44 Å, whereas the O14 carbonyl oxygen of the NAD-ad phosphoester intermediate is at a distance of 2.48 Å. Furthermore, the GluA162 Oε2 atom is 3.44 Å from M^+(II) and AspA220 makes a strong salt bridge with M^+(II), the distance between the AspA220 Oδ2 atom and M^+(II) being 2.54 Å (Figure 4). Overall, *B. subtilis* NAD^+ synthetase can be considered as having a cluster built of two Mg^{2+} ions, one M^+ cation plus an ammonium ion, in the active site. The distances between pairs of neighbouring cations range from 4.32–4.81 Å. Moreover, the four cations do not belong to the same plane, but rather tend to be clustered in a sort of chair-like configuration, as shown in Figure 4.

Discussion

Although the catalytic mechanism of NAD^+ synthetase was previously investigated to a certain extent [6,11], a number of key questions regarding the general catalytic strategy adopted by the enzyme remained to be answered. In particular, the exact locations of deamido-NAD^+ and of the ammonia-binding sites, together with the involvement of specific protein residues and Mg^{2+} ions in catalysis, were unknown. The high-resolution three-dimensional structure of the NAD-ad trapped intermediate and the structural studies of the cation-binding sites reported in this study allow us to trace a more precise picture of the entire reaction carried out by the enzyme.

As described above, we observe two NAD-ad molecules in the dimeric enzyme efficiently filling the enzyme active site, which consists of a long cleft connecting the ATP and deamido-NAD^+ binding sites (Figures 2 and 5). As shown in Figure 2, the two NAD-ad molecules adopt an elongated conformation, roughly perpendicular to the homodimer molecular dyad. Interestingly, each NAD-ad molecule displays an internal quasi-twofold axis relating the two adenosyl moieties present in the intermediate. Such an approximate local twofold axis is located between the nicotinic ring and the deamido-NAD^+ β-phosphate, perpendicular to the enzyme molecular dyad (Figures 2 and 6). It can be seen that the enzyme recognizes two substrates, deamido-NAD^+ and ATP, both of which contain a common adenosyl-diphosphate fragment. In NAD^+ synthetase, the mononucleotidic substrate (ATP) is bound at the classical topological switch point, where a dinucleotide is usually observed in Rossmann-fold-based NAD(P)-binding proteins [19], and a new dinucleotide-binding site is present. Such structural organization could be related to the different chemical involvement of the dinucleotide in different enzymes, such as a substrate in NAD^+ synthetase and a redox cofactor in dehydrogenases. In this respect, a new NAD^+-binding site and an unusual NAD^+ conformation

Figure 5

Stereoview of the catalytic center in NAD+ synthetase, including the ATP-binding site (lower) and the deamido-NAD+ binding site (upper). The entire NAD-ad molecule (AMP and deamido-NAD+ moieties on the lower and upper sides, respectively), PP_i and two Mg^{2+} ions are shown. Color coding is as described in Figures 2 and 3. This figure was generated using MOLSCRIPT [43].

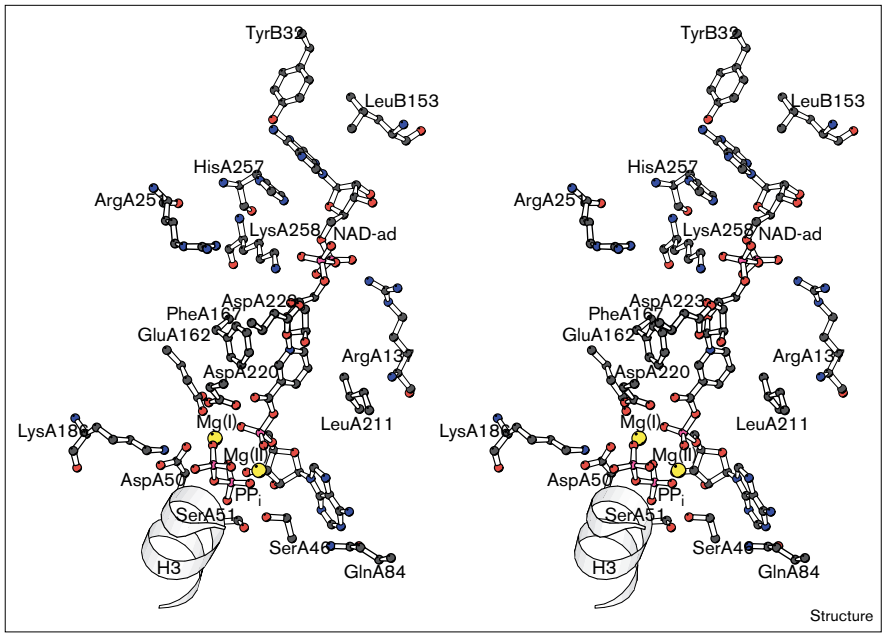

have also been reported in diphtheria toxin, which uses NAD+ as labile substrate [20]. The dinucleotide conformations observed in the two enzymes are unrelated, however; the nicotinic ring is in the *anti* orientation and the nicotinic mononucleotide portion adopts an extended conformation in NAD+ synthetase, whereas a *syn* orientation of the nicotinamide ring and a highly folded conformation of the nicotinamide mononucleotide portion are present in diphtheria toxin [20].

Several enzymes, including tRNA synthetases, coenzyme A ligases, luciferase, peptide synthetases and asparagine synthetase, are known to form adenylate intermediates as a common strategy for substrate activation [27–30]. Amongst them, aminoacyl-tRNA synthetases have been characterized extensively. It has been reported that a general mechanism for the adenylation step in different class II tRNA synthetases may involve conserved arginine residues and two or three divalent cations, which have been proposed to stabilize the pyrophosphate leaving group and the pentacoordinate transition-state intermediate formed during adenylation [31,32]. Moreover, it has been shown that in *Escherichia coli* asparagine synthetase, Arg325 is fundamental in the stabilization of the pentacovalent transition state leading to the formation of β-aspartyl-AMP [33].

The NAD+ synthetase E–NAD-ad complex reveals two Mg^{2+} ions interacting with the α-phosphate of the AMP portion and with both PP_i phosphates. They are located on either side of the PP_i unit, and are also coordinated to the α-phosphate oxygen atoms (Figure 3c). Inspection of the protein matrix surrounding the nicotinic ring and the AMP α-phosphate moieties in the NAD-ad, does not reveal any protein sidechain properly positioned to interact directly with the α-phosphate as a potential stabilization of the pentacovalent transition-state intermediate formed during the first step of the catalyzed reaction (Figures 1, 5 and 7). On the other hand, the two divalent cations accompanying the pyrophosphate molecule not only neutralize the PP_i unit negative charges but also, as Lewis acids, increase the electrophilic character of the AMP α-phosphate through polarization. Hence, transferring the structural observations about the AMP moiety of NAD-ad and the PP_i pair to the mechanistic view of the ATP hydrolysis, the Mg^{2+} ions may participate in weakening the ATP α–β phosphate bond and, more importantly, they may stabilize the negative charge carried by the pentacovalent transition-state intermediate. Thus, a major contribution towards enhancing the adenylation reaction rate could be provided by the magnesium cations.

Several protein residues participate in structuring the active site for substrate recognition and provide the binding energy essential for catalysis. Amongst them, AspA173 is the main structural determinant in defining the orientation of deamido-NAD+ carboxylate for an efficient nucleophilic attack on the electrophilic ATP α-phosphate (Figures 4, 5 and 7). The general strategy employed by NAD+ synthetase, to assist the first step of the catalyzed reaction, does not seem to rely on the direct use of protein sidechains. Rather, the entire catalytic power is likely to be provided by the two Mg^{2+} ions and, as

Figure 6

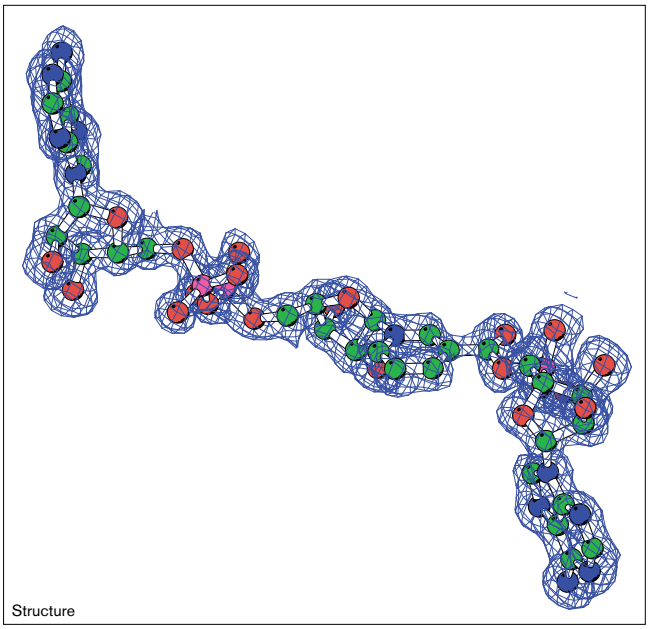

Final electron density omit map at 1.3 Å resolution, for the NAD-ad intermediate. The intermediate is viewed perpendicular to its internal quasi-twofold axis relating the two adenosyl moieties. Color coding is as described in Figure 2. This figure was generated using MOLSCRIPT [43].

described below, by one of the monovalent cations observed in the ATP-binding site.

Once the NAD-ad intermediate is formed, the nucleophilic attack of an ammonia molecule yields the final product, NAD^+, and releases AMP. In order to investigate this second step of the catalyzed reaction, and in search of the ammonia-binding site, we have determined the structure of the E–ATP–Tl^+ complex. As described above, two major monovalent cation-binding sites were observed. One of them, M^+(II), is located next to the PP_i and AMP fragments, whereas its position is occupied by the solvent molecule W339 in the structure of the E–NAD-ad complex (Figure 4). Amongst the interactions established by M^+(II) with the molecular environment, those with PP_i further stabilize the negatively charged leaving group. The electrostatic interactions with the α-phosphate group and with the NAD-ad O14 carbonyl oxygen enhance the electrophilicity of the NAD-ad C20 atom, which will be attacked by the incoming ammonia molecule (Figures 4 and 7). Furthermore, the pentacovalent and tetrahedral transition states formed during the first and second steps, respectively, of the catalyzed reaction, could both be stabilized through electrostatic interactions with M^+(II). As described for Mg^{2+} cations, and also for M^+(II), the proposed catalytic role is not merely an electrostatic stabilization of substrates and leaving group, but also an active participation in the reaction via the polarization of reacting atoms (the α-phosphate and the carbon atom of the phosphoester intermediate during the first and the second step, respectively) and a possible stabilization of the transition states.

The second monovalent cation — M^+(II) — is located in a negatively charged pocket, which is most likely to represent an ammonium-ion-binding site. In fact, both the coordination of M^+(II) and, more notably, its location with respect to the NAD-ad nicotinic C20 atom support this hypothesis (Figures 4 and 7). This finding suggests that an ammonium ion initially binds to a negatively charged pocket in NAD^+ synthetase before the reactive ammonia, delivered *in situ* upon deprotonation of the ammonium ion, acts as the incoming base to complete the catalytic reaction. It can be seen that AspA173 (making a strong salt bridge with the ammonium ion) is well positioned both to perform proton abstraction on the bound ammonium and to stabilize the positively charged amino group of the tetrahedral transition-state intermediate (Figure 4). The configuration of this negatively charged pocket may favour selective binding of an ammonium ion versus a water molecule, determining the nature of the products. In fact, if a water molecule were to attack the NAD-ad intermediate, the whole enzymatic reaction would yield deamido-NAD^+ and AMP, whereas if the nucleophile is an ammonia molecule, NAD^+ and AMP are formed. Thus, the presence of an ammonium-binding site allows the reaction to be carried out in aqueous solution.

Inspection of the solvent structure in the E–NAD-ad adduct, which is particularly reliable because of the high resolution of this study, reveals a possible pathway for the ammonium from the protein surface to the catalytic heart of NAD^+ synthetase. Indeed, five water molecules, located at mutual hydrogen-bonding distances, connect the protein surface to the proposed ammonium-binding site. Starting from the solvent side, we observe the following sequence: W790-W366-W344-W388-W559; W559 occupies the ammonium-binding site in the NAD-ad complex (Figure 8). Water W344 is located in the narrowest section of the channel, hydrogen bonded to the carbonyl oxygen atom of AspA173 (2.77 Å) on one side, and to the mainchain nitrogen atom of ThrA157 (2.92 Å) on the other side (Figure 8). It has been previously reported that the mutation Gly156→Glu yields an enzyme 200-times less active than the wild-type species, mainly affecting the ammonium K_m value [6]. This observation is in keeping with our proposal for the ammonium ion pathway to the catalytic site: replacement of a glycine with a negatively charged glutamate residue at position 156 would lead to the formation of an ion pair between the glutamate residue and the ammonium cation, along its pathway from the protein surface to the catalytic site. In fact, modeling of Glu156, whose Cα is at a distance of 3.52 Å from W344, places its carboxylate group 2.7 Å from W344 and 3.1 Å from W388; W344 and

Figure 7

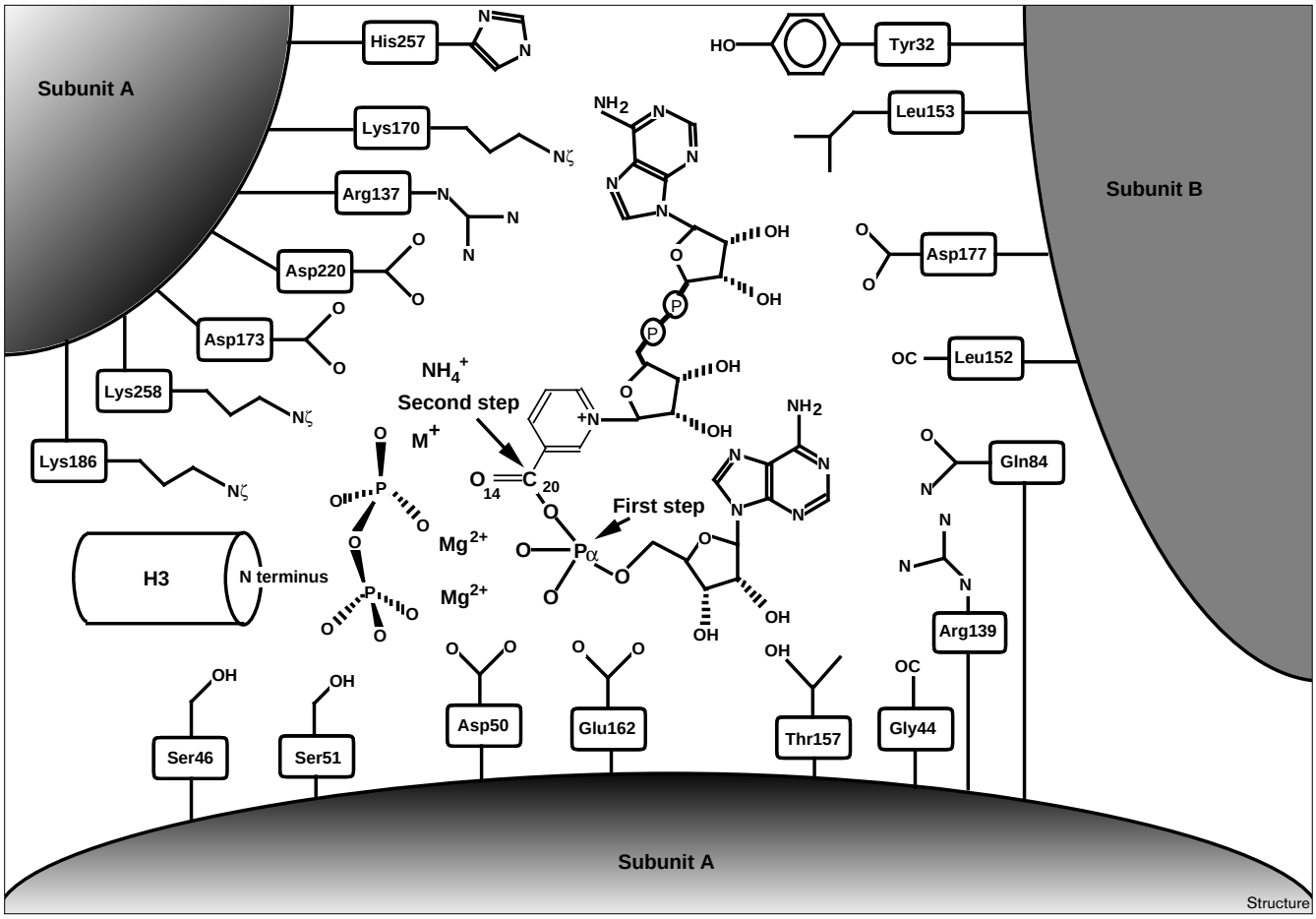

A schematic representation of the interactions involved in NAD-ad, PP_i, Mg^{2+}, M^+(II) and NH_4^+ (reported as M^+(I) in the text) binding. Key atoms for the first and second steps of the catalyzed reaction, are indicated by an arrow.

W388 are two of the solvent molecules that trace the proposed ammonium pathway in the structure of the E–NAD-ad complex (Figure 8).

Hence, in the strictly ammonia-dependent *B. subtilis* NAD+ synthetase, the binding species is proposed to be an ammonium cation that travels from the bulk solvent to

Figure 8

Stereoview of the proposed ammonium pathway in NAD+ synthetase. W559 occupies the ammonium-binding site in the structure of the E–NAD-ad complex. The mutation Gly156→Glu is indicated. Color coding is as described in Figures 2 and 3. This figure was generated using MOLSCRIPT [43].

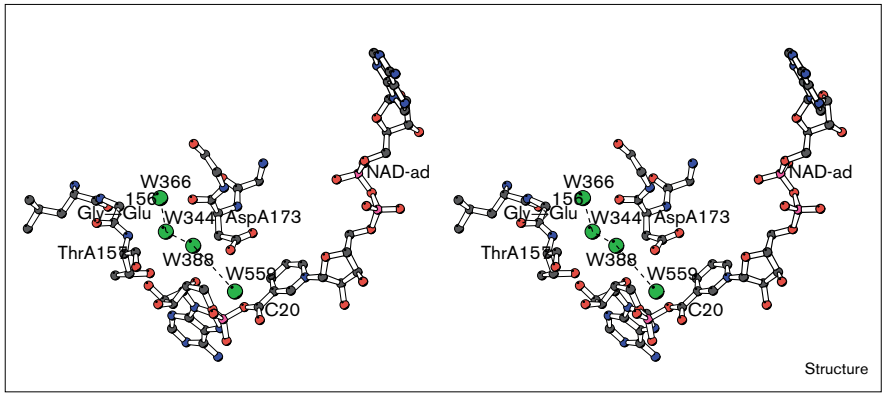

the active site through a fully solvent-accessible channel. It has been reported recently for two other amidotransferases (PRPP amidotransferase and carbamoyl phosphate synthetase, which are both able to use glutamine as a nitrogen source) that activation of the enzyme upon substrate binding opens a long solvent-inaccessible channel, which connects the glutamine-hydrolysis domain to the synthase domain, thereby allowing ammonia transfer between the two catalytic sites [13,34]. Here, we show that *B. subtilis* NAD^+ synthetase hosts an ammonium-binding site, suggesting a different behaviour for the enzyme compared with PRPP amidotransferase and carbamoyl phosphate synthetase.

A notable feature of the E–NAD-ad complex is represented by the presence of the pyrophosphate molecule, the leaving group of the first step of the catalyzed reaction, in the active site. Because the NAD-ad intermediate is expected to be very unstable in solution, its escape from the active site has to be avoided. A possible way for the enzyme to perform this task is by the closure of the active site once the first step of the catalyzed reaction is completed. In this respect, it was reported previously that two polypeptide segments (residues 82–87 and 204–225) are disordered in the free enzyme and become fully structured upon ATP binding, acting as a partial lid to the ATP-binding site ([11]; Figure 2). Remarkably, the O3γ O atom of the PP_i unit is engaged in a hydrogen bond with the ThrA208 mainchain nitrogen atom (3.11 Å), a residue belonging to one of the two mobile loops that become structured upon substrate binding (Figures 2 and 3b). Thus, PP_i participates in fixing the conformation of these two loops, which, in turn, may prevent or contain the loss of the NAD-ad intermediate from the active site. The enzyme is trapped in this locked state until the ammonia molecule carries out the final step of the reaction. Our structural data suggests that product release can take place only after all the substrates are bound to the enzyme, and product release is ultimately controlled by the conformation adopted by the two mobile loops.

The emerging picture for the catalytic mechanism in *B. subtilis* NAD^+ synthetase consists of two distinct strategies adopted in the two different steps of the catalyzed reaction (Figures 1 and 7). During the formation of NAD-ad, the enzyme seems to be providing only a well-suited active-site configuration, fixing the conformations of the reactant groups. But the catalysis is carried out solely with the assistance of an electron-withdrawing trimetallic constellation present in the active site (two Mg^{2+} ions and one monovalent cation). Indeed, no direct interactions are observed between the α-phosphate and any protein residues, and stabilization of the intermediate pentacovalent transition state is likely to be determined mainly by the cation cluster. A similar situation is observed for the phosphoryl transfer reactions catalyzed by RNAs, such as *Tetrahymena* group I intron, RNase P and hammerhead ribozyme, for which a major contribution of coordinated active-site divalent cations for efficient catalysis was demonstrated ([35] and references therein). Such a fundamental property of catalytic RNAs also seems to act in *B. subtilis* NAD^+ synthetase, hinting at a conservation of mechanisms during the transition from RNA-based to protein-based enzymes.

A different behavior is observed for the second step of the overall reaction, the transformation of NAD-ad into NAD^+, releasing AMP. In this case, the protein matrix is not only orienting and stabilizing the reactant species, but also directly intervening in the catalytic process. In this respect, AspA173 is a key residue in the recognition of the primarily bound ammonium cation in its subsequent deprotonation and in the stabilization of the tetrahedral transition-state intermediate.

Biological implications

Nicotinamide adenine dinucleotide (NAD^+) is important in metabolism, not only for shuttling redox equivalents within the metabolic network of the cell, but also for its direct involvement in a number of fundamental processes, such as DNA repair, DNA recombination and protein–ADP ribosylation. Thus, it is self-evident that control and regulation of the NAD^+ levels is crucial in every living organism. The ubiquitous enzyme NAD^+ synthetase therefore catalyzes a key step in cellular metabolism the last step in NAD^+ biosynthesis.

NAD^+ synthetase belongs to the extensively studied amidotransferase family and is a member of the N-type ATP pyrophosphatases, which have been suggested recently to be evolutionarily related to phosphadenylyl sulfate reductases and ATP sulphurylases.

Interestingly, in the strictly NH_3-dependent *Bacillus subtilis* NAD^+ synthetase the ATP-binding site is located at the classical α/β topological switch point (where a dinucleotide is usually observed in a Rossmann-fold-based NAD(P)-binding protein) and a novel deamido-NAD^+-binding site is present. We speculate that such structural organization could be related to the that fact that, in NAD^+ synthetase, deamido-NAD^+ behaves as a labile substrate and not as a redox cofactor.

We suggest that the catalytic strategy adopted during the adenylation step (the first step of the catalyzed reaction), does not rely on the direct involvement of any protein residues, and is likely to be carried out by the essential contribution of the binding energy and with the fundamental assistance of the electron-withdrawing trimetallic constellation present in the active site. The essential involvement of the cations in NAD^+ synthetase resembles the behavior in the phosphoryl

transfer reaction catalyzed by RNAs, suggesting a conservation of catalytic mechanism during the transition from RNA-based to protein-based enzymes.

We discovered that *B. subtilis* NAD+ synthetase hosts an ammonium-binding site. Asp173 is a key residue in both the deprotonation of the primarily bound ammonium ion and the stabilization of the tetrahedral transition-state intermediate. Thus, in the second step of the catalyzed reaction, we observe a direct intervening in the catalysis of protein residues. Moreover, in keeping with previously reported biochemical studies on the Gly156→Glu mutant, a solvent-accessible channel is proposed to represent the ammonium pathway from the bulk solvent to the catalytic heart of NAD+ synthetase.

The presence of the PP_i leaving group in the active site suggests that product release can take place only after all substrates are bound to the enzyme, and that product release is ultimately controlled by the conformation adopted by two mobile loops, which behave as entire domains in complex enzymes.

Materials and methods

Crystallization

Crystals of the E–ATP complex were grown from solution containing 22% v/v PEG 400, 0.05 M $MgCl_2$, 0.1 M sodium acetate, pH = 5.2, as previously described [11]. Crystals of the E–NAD-ad complex were obtained by co-crystallization, using the hanging drop vapour diffusion technique. Protein droplets at 15 mg/ml, containing 5 mM ATP and 20 mM NAD^+, were equilibrated against mother liquor solution containing 22% PEG 400, 0.1 M sodium acetate, 0.05 M $MgCl_2$, pH = 5.2 at T = 20°C. The E–ATP–Tl^+ and E–ATP–Mn^{2+} adducts were prepared soaking crystals of the E–ATP complex in their mother liquor, saturated with thallium acetate for E–ATP–Tl^+ and replacing $MgCl_2$ with $MnCl_2$ in the crystallization solution for E–ATP–Mn^{2+}. Crystals were soaked for 24 h prior to data collection. All crystals are isomorphous to the E–ATP crystals, belong to space group P21 with cell dimensions $a = 53.3$ Å, $b = 87.8$ Å, $c = 61.4$ Å, $\beta = 110.6°$, and contain one NAD^+ synthetase dimer in the asymmetric unit.

Data collection

Diffraction data of the E–NAD-ad complex were collected on a flash-cooled crystal, using synchrotron radiation at the beam line BW7B at EMBL/DESY (Hamburg, Germany; $\lambda = 1.0$ Å), on a MAR research image plate area detector. Crystals were transferred for a few seconds in a solution containing 25% PEG 400, 0.1 M sodium acetate, 0.05 M $MgCl_2$, 0.005 M ATP, 0.020 NAD^+, pH 5.2 and 15% glycerol, as a cryoprotectant, mounted on a thread loop and flash-frozen at 100K under a nitrogen stream.

Data collection up to 2.5 Å resolution, for the E–ATP–Tl^+ and E–ATP–Mn^{2+} adducts, was carried out at room temperature, using a Rigaku rotating anode RU200 (CuKα, $\lambda = 1.5418$ Å), running at 50 kV, 180 mA, equipped with an R-AXIS II image plate area detector.

Synchrotron data were integrated, scaled and merged using DENZO and SCALEPACK [36], whereas the intensities collected in house were evaluated using the program MOSFLM [37], and the CCP4 suite [38]. Table 1 gives a summary of the data-collection statistics.

Table 1

Data collection and refinement statistics.

Data	
Resolution (Å)	20.0–1.3
No. of observations	333,971
No. of unique reflections	111,493
Completeness (%)	92.0
*R_{merge} (%)	3.4
Model refinement	
No. of protein atoms	4285
No. of water molecules	495
No. of Mg^{2+} sites	4
No. of nucleotides	2
No. of pyrophosphate molecules	2
No. of glycerol molecules	2
†R factor (%)	15.5
‡R free (%)	18.0
Mean B value for sidechain (Å^2)	18.4
Mean B value for mainchain (Å^2)	13.5
Rms deviations from ideality	
bond lengths (Å)	0.019
bond lengths (Å)	0.033
planar 1–4 distance (Å)	0.039
§ΔCα (Å)	0.4
Ramachandran outliers	0

*$R_{merge} = \Sigma | Ii - < Ii > | / \Sigma < Ii >$, where $< Ii >$ is the mean value of the ith intensity measurements. †R factor $= \Sigma | F_{obs} - F_{calc} | / \Sigma | F_{obs} |$. ‡R free $= \Sigma | F_{obs} - F_{calc} | / \Sigma | F_{obs} |$ (for the selected portion of all data). §Rms deviation for all Cα atoms after superposition of the two noncrystallographically related subunits.

Crystallographic refinement

For the crystallographic refinement, the coordinates of the E–ATP complex (PDB code 1nsy) were used as the initial model, excluding the Mg^{2+}, AMP, ATP and PP_i moieties and the solvent molecules. The crystallographic refinement was performed in the 20.0–1.3 Å resolution range, using the REFMAC program [39], with the Engh–Huber stereochemical parameters [40], and minimizing against a maximum likelihood function. Neither NCS restraints nor structure factor sigma cutoff were applied.

A total of 1114 reflections were randomly chosen for the evaluation of the free R factor [41]. After the R actor fell to a value of 0.23, calculated $3F_o–2F_c$ and $2F_o–2F_c$ electron-density maps allowed an unambiguous interpretation of the electron density. Two molecules of NAD-ad, two PP_i, four Mg^{2+} and two glycerol molecules (the cryoprotectant) were fitted in the enzyme dimer. Moreover, a total of seven sidechains were refined in double conformations: SerA15, GluA21, SerA102, GluA256, SerB15, SerB115 and GluB150. Solvent molecules were manually added at positions with density $> 3\sigma$ in the $2F_o–2F_c$ map, considering only peaks engaged in at least one hydrogen bond with a protein or a solvent atom.

This model was then subjected to several cycles of refinement using REFMAC, until convergence, including hydrogen atoms at calculated positions. Convergence was reached at an R factor of 0.155 and a free R factor of 0.180, in the 20.0–1.3 Å resolution range. The final model consists of 4285 protein atoms (542 residues), 495 water molecules, two PP_i ions, two NAD-ad molecules, four Mg^{2+} ions and two glycerol molecules. The average B factor for the protein atoms was 15.0 Å^2 for A chain (12.8 Å^2 for mainchain and 17.36 Å^2 for sidechain) and 17.0 Å^2 for B chain (14.2 Å^2 for mainchain and 19.3 Å^2 for sidechain). The mean B value for solvent atoms was 24.0 Å^2. The overall quality of

the structure has been assessed with the program PROCHECK [42]; 96% of the amino acid residues are in the most favored regions of the Ramachandran plot and no outliers are present. Details of the refinement statistics are given in Table 1.

Accession numbers

The atomic coordinates of the NAD-ad complex (E–NAD-ad) have been deposited with the Protein Data Bank (accession code 2nsy).

Acknowledgements

The authors would like to thank A Mattevi, G Valentini, M Fraaije, A Galizzi (University of Pavia) and P Ascenzi (Third University of Rome) for several helpful discussions. A Tarricone (University of Torino, Italy), V Lamzin (EMBL Hamburg, Germany) and K Wilson (York University, UK) are greatly acknowledged for precious help during the protein purification, the data collection and the refinement steps, respectively. This research was supported in part by grants from the Agenzia Spaziale Italiana (contract number ASI-ARS-96-191/114) and National Tuberculosis Project (Istituto Superiore di Sanità - Ministero della Sanità; contract number 96/D/T49). We thank the European Union for support of the work at EMBL Hamburg, through the HCMP to Large Installation Project (contract CHGE-CT93-0040) and Advanced Methods for Crystallography of Biological Macromolecules (contract number CT940690).

References

1. Foster, J.W. & Moat, A.G. (1980). Nicotinamide adenine dinucleotide biosynthesis and pyridine nucleotide cycle metabolism in microbial system. *Microbiol. Rev.* **44**, 83-105.
2. White, H.B. (1982). Biosynthetic salvage pathways of pyridine nucleotide coenzymes. In *Pyridine Nucleotide; Coenzyme.* (Everse, J., Anderson, B.M. & You, K.S., eds), pp. 1-17, Academic Press Inc., New York, USA.
3. Tritz, G.J. (1987). NAD biosynthesis and recycling. In *Escherichia coli and Salmonella typhimurium Cellular and Molecular Biology.* (Neidhardt, F.C., *et al.*, & Umbarger, H.E., eds), Vol. 1, pp. 557-563, American Society for Microbiology, Washington DC, USA.
4. Spencer, R.L. & Preiss, J. (1967). Biosynthesis of diphosphopyridine nucleotide: the purification and the properties of diphosphopyridine nucleotide synthetase from *Escherichia coli. J. Biol. Chem.* **242**, 385-392.
5. Caramori, T., Calogero, S., Albertini, A. & Galizzi, A. (1993). Functional analysis of the *outB* gene of *Bacillus subtilis. J. Gen. Microbiol.* **139**, 31-37.
6. Nessi, C., Albertini, A.M., Speranza, M.L. & Galizzi, A. (1995). The outB gene of *Bacillus subtilis* codes for NAD synthetase. *J. Biol. Chem.* **270**, 6181-6185.
7. Antelmann, H., Schmid, R. & Hecker, M. (1997). The NAD synthetase NadE (outB) of B*acillus subtilis* is a σ^B-dependent general stress protein. *FEMS Microbiol. Lett.* **153**, 405-409.
8. Zalkin, H. & Smith, J.L. (1998). Enzymes utilizing glutamine as an amide donor. *Adv. Enzymol. Relat. Areas Mol. Biol.* **72**, 87-144.
9. Smith, L.J., *et al.*, & Satow, Y. (1994). Structure of the allosteric regulatory enzyme of purine biosynthesis. *Science* **264**, 1427-1433.
10. Tesmer, J.G., Klem, T.J., Deras, M.L., Davisson, V.J. & Smith, J. (1996). The crystal structure of GMP synthetase reveals a novel catalytic triad and is a structural paradigm for two enzyme families *Nat. Struct. Biol.* **3**, 74-86.
11. Rizzi, M., *et al.*, & Galizzi, A. (1996). Crystal structure of NH_3-dependent NAD synthetase from *Bacillus subtilis. EMBO J.* **15**, 5125-5134.
12. Isupov, M.N., *et al.*, & Teplyakov, A. (1996). Substrate binding is requires for the assembly of the active conformation of the catalytic site in Ntn amidotransferases: evidence from the 1.8 Å crystal structure of the glutaminase domain of glucosamine 6-phosphate synthase. *Structure* **4**, 801-810.
13. Thoden, J.B., Holden, H.M., Wesenberg, G., Raushel, F.M. & Rayment, I. (1997). Structure of carbamoyl phosphate synthetase: a journey of 96 Å from substrate to product. *Biochemistry* **36**, 6305-6316.
14. Nakatsu, T., Kato, H. & Oda, J. (1998). Crystal structure of asparagine synthetase reveals a close evolutionary relationship to class II aminoacyl-tRNA synthetase. *Nat. Struct. Biol.* **5**, 15-19.
15. Cantoni, R., Branzoni, E., Labò, M., Rizzi, M. & Riccardi, G. (1998). The MTCY428.08 gene of Mycobacterium tuberculosis codes for NAD synthetase. *J. Bacteriol.* **180**, 3218-3221.
16. Zerez, C.R., Wong, M.D. & Tanaka, K.R. (1990). Partial purification and properties of nicotinamide adenine dinucleotide synthetase from human erythrocytes: evidence that enzymatic activity is a sensitive indicator of lead exposure. *Blood* **75**, 1576-1582.
17. Wagner, R. & Wagner, K.G. (1985). The pyridine-nucleotide cycle in tobacco. Enzyme activities for the de-novo synthesis of NAD. *Planta* **165**, 532-537.
18. Savage, H., Montoya, G., Svensson, C., Schwenn, J.D. & Sinning, I. (1997). Crystal structure of phosphoadenylyl sulphate (PAPS) reductase: a new family of adenine nucleotide α hydrolases. *Structure* **5**, 895-906.
19. Carugo, O. & Argos, P. (1997). NADP-dependent enzymes. I: conserved stereochemistry of cofactor binding. *Proteins* **28**, 10-28.
20. Bell, C.E., Yeates, T.O. & Eisenberg, D. (1997). Unusual conformation of nicotinamide adenine dinucleotide (NAD) bound to diphtheria toxin: a comparison with NAD bound to the oxidoreductase enzymes. *Protein Sci.* **6**, 2084-2096.
21. Brenner, S.E., Chothia, C., Hubbard, T.J.P. & Murzin, A.G. (1996). Understanding protein structure: using SCOP for fold interpretation. *Methods Enzymol.* **266**, 635-643.
22. Rossmann, M.G., Liljas, A., Branden, C.I. & Banaszak, L.J. (1975). Evolutionary and structural relationships among dehydrogenases. In *The Enzymes.* (Boyer, P.D., ed.), pp. 61-102, Academic Press, New York.
23. Carugo, O., Djinovic, K. & Rizzi, M. (1993). Comparison of the coordinative behaviour of calcium (II) and magnesium (II) from crystallographic data. *J. Chem. Soc. Dalton Trans.* 2127-2135.
24. Zalkin, H. (1985). NAD synthetase. *Methods Enzymol.* **113**, 297-302.
25. Liaw, S.H., Kuo, I. & Eisenberg, D. (1995). Discovery of the ammonium substrate site on glutamine synthetase, a third cation binding site. *Protein Sci.* **4**, 2358-2365.
26. Liaw, S.H. & Eisenberg, D. (1994). Structural model for the reaction mechanism of glutamine synthetase, based on five crystal structures of enzyme-substrate complexes. *Biochemistry* **33**, 675-681.
27. Delarue, M. (1995). Aminoacyl-tRNA synthetase. *Curr. Opin. Struct. Biol.* **5**, 48-55.
28. McElroy, W.D., DeLuca, M. & Travis, J. (1967). Molecular uniformity in biological catalysis. The enzymes concerned with firefly luciferin, amino acid, and fatty acid utilization are compared. *Science* **157**, 150-160.
29. Conti, E., Franks, N.P. & Brick, P. (1996). Crystal structure of firefly luciferase throws light on a superfamily of adenylate-forming enzymes. *Structure* **4**, 287-298.
30. Conti, E., Stachelhaus, T., Marahiel, M.A. & Brick, P. (1997). Structural basis for the activation of phenylalanine in the non-ribosomal biosynthesis of gramicidin S. *EMBO J.* **16**, 4174-4183.
31. Arnez, J.G., Augustine, J.G., Moras, D. & Francklin, C.S. (1997). The first step of aminoacylation at the atomic velev in histidyl-tRNA synthetase. *Proc. Natl Acad. Sci. USA* **94**, 7144-7149.
32. Belrhali, H., *et al.*, & Cusack, S. (1995). The structural basis for seryl-adenylate and Ap4A synthesis by seryl-tRNA synthetase. *Structure* **3**, 341-352.
33. Boehlein, K.S., Walworth, E.S., Richards, N.G.J. & Schuster, S.M. (1997). Mutagenesis and chemical rescue indicate residues involved in β-aspartyl-AMP formation by *Escherichia coli* asparagine synthetase. *J. Biol. Chem.* **272**, 12384-12392.
34. Krahn, J.M., *et al.*, & Smith, J.L. (1997). Coupled formation of an amidotransferase interdomain ammonia channel and a phosphoribosyltransferase active site. *Biochemistry* **36**, 11061-11068.
35. Narkilar, G.J. & Herschlag, D. (1997). Mechanistic aspects of enzymatic catalysis: lessons from comparison of RNA and protein enzymes. *Annu. Rev. Biochem.* **66**, 19-59.
36. Otwinowski, Z. & Minor W. (1997). Processing of X-ray diffraction data collected in oscillation mode. *Methods Enzymol.* **276**, 307-326.
37. Leslie, A.G.W. (1992). *Jnt CCP4 and ESF-EACMB Newslett. Protein Crystallogr.* No. 26. Warrington: Daresbury Laboratory, UK.
38. Collaborative Computational Project Number 4. (1994). The CCP4 suite: programs for protein crystallography. *Acta Crystallogr. D* **50**, 760-767.
39. Murshudov, G.N., Vagin, A.A. & Dodson, E.J. (1997). Refinement of macromolecular structures using the maximum-likelihood method. *Acta Crystallogr. D* **53**, 240-255.
40. Engh, R.A. & Huber, R. (1991). Accurate bond angles and parameters for X-ray protein structure refinement. *Acta Crystallogr. A* **45**, 392-400.
41. Brunger, A.T. (1992). The free R value: a novel statistical quantity for assessing the accuracy of crystal structure. *Nature* **355**, 472-474.
42. Laskowski, R.A., Mac Arthur M.W., Moss, D.S. & Thornton, J.M. (1993). PROCHECK: a program to check the stereochemistry of protein structures. *J. Appl. Crystallogr.* **26**, 283-291.
43. Kraulis, P.J. (1991). MOLSCRIPT: a program to produce both detailed and schematic plots for protein structures. *J. Appl. Crystallogr.* **24**, 946-950.